PHYSICAL REVIEW B

CONDENSED MATTER

THIRD SERIES, VOLUME 39, NUMBER 5 15 FEBRUARY 1989-I

Experimental Fermi surface of Mo(011)

K. Jeong, R. H. Gaylord,* and S. D. Kevan

Department of Physics and Materials Science Institute, University of Oregon, Eugene, Oregon 97403-1274

(Received 29 August 1988)

High-resolution angle-resolved photoemission results are presented which allow us to determine the complete Fermi surfaces for the surface-localized electronic levels on the clean and hydrogen-covered Mo(011) surfaces. Similar to previously presented data for W(011), we observe a total of three distinct closed hole orbits and one closed electron orbit. The hole orbits are elliptical and are centered on different projections of the same bulk Fermi-surface ellipsoid. They are located at the center and along each of the edges of the surface Brillouin zone. The surface electron pocket is closed but has a very complex shape which is somewhat different from the one observed on W(011). It orbits the projection of a bulk electron pocket which is traditionally called a jack, and is centered in the surface Brillouin zone. As was observed for W(011), these orbits are affected to different extents by hydrogen adsorption. The hole pockets are rapidly quenched by hydrogen, while the electron pocket grows in area until it merges with its image in the second Brillouin zone. At saturation there exist two hole pockets which are the remnants of the clean-surface electron pocket. These results are discussed in terms of the dynamical response of the surface. Electronic damping mechanisms for low-energy surface excitations are discussed. Some of the possible vibrational Kohn anomalies are enumerated.

I. INTRODUCTION

The Fermi surface in crystalline metallic systems is of fundamental importance since it determines many macroscopic and microscopic properties. Starting from Fermi-surface contours, observables such as heat capacities, transport behavior, and intraband optical properties can be predicted. In addition, issues relating to phase stability and phonon behavior can be partially understood. For these reasons, several techniques have been developed and applied to study the Fermi surfaces of bulk, three-dimensional media. This work has produced a useful data base which the solid-state-physics community can utilize.[1]

It is surprising that more experimental and theoretical attention has not been focused on the determination of complete Fermi surfaces of two-dimensional (2D) and quasi-2D systems. The lowered dimensionality of these systems leads to Fermi surfaces which are well approximated as being tubular in shape. This geometry leads to more effective coupling of different portions of the Fermi surface and thus to more pronounced instabilities and electronic screening anomalies. These anomalies can in principle have a very pronounced effect on lattice stability. For example, this is the supposed mechanism for many of the distortions observed in quasi-2D layered materials.[2] The role of Fermi-surface nesting in driving reconstructions observed on nominally clean surfaces was predicted nearly a decade ago.[3] Interest has recently been revived in this subject by theoretical work on Mo(001).[4]

Where the Fermi-surface anomalies are not strong enough to produce reconstruction at a given temperature, there can be enhanced, momentum-dependent coupling of the electron-hole–pair continuum to phonons and other low-energy excitations in the system. These couplings are manifested by Kohn anomalies in the appropriate dispersion relations.[5] A Kohn anomaly may be conveniently viewed as a precursor to a broken symmetry (e.g., a soft phonon) which may in fact set in under appropriate circumstances. Their existance is intimately related to force constants, and thus to the dynamical behavior of the lattice. Alternatively, a Kohn anomaly can be viewed as a manifestation of enhanced electronic damping of a low-energy excitation, and thus provides a mechanism whereby energy can be transferred and dissipated into electronic degrees of freedom. Such effects are of central importance in understanding the dynamical behavior of surfaces.[6] To date, there have been two experimental reports of anomalies in surface-phonon dispersion relations which were attributed to Fermi-surface coupling.[7,8] Work such as that reported here should motivate further efforts along these lines.

Part of the reason that Fermi surfaces of 2D systems

have not received more experimental attention is that the techniques traditionally used to study 3D systems, de Haas–van Alphen, magnetoacoustic, and magnetoresistance measurements, are not readily applied. These generally lack the required sensitivity to observe an individual 2D interface or are unable to discriminate the generally larger bulk signal. In addition, they require a material of higher perfection than is routinely attained by current interface preparation procedures. An alternative technique for determining the Fermi surface in any dimension is angle-resolved photoemission (ARP).[9–11] While the accuracy of this technique in determining the Fermi surface of a 3D system is not adequate for it to compete with those mentioned above, it is the technique of choice for nominally clean surfaces. ARP was first applied in the determination of a complete, 2D Fermi surface several years ago.[12] The goal in that study was to understand the driving force for the observed clean W(001) surface reconstruction. The more or less negative conclusions derived ended further efforts.

Given the general significance of Fermi surfaces of 2D systems outlined above, a comprehensive and systematic study of many different clean and adsorbate-covered surfaces should be useful. Recently, we reported our initial measurements of the Fermi surface of clean and hydrogen-covered W(011).[13] Here, we give similar results for Mo(011). These two metals have the same structure and nearly identical lattice constants. A schematic of the body-centered-cubic (011) surface unit net is given in Fig. 1 along with the surface and bulk Brillouin zone.

The two (011) surfaces are interesting as much for their differences as for their similarities. For example, W(011) has been observed to reconstruct upon hydrogen adsorption via a uniform lateral shift along the $[01\bar{1}]$ direction of the surface layer relative to the second layer.[14,15] As is apparent from Fig. 1, this reconstruction changes some nearest-neighbor bond angles but not bond lengths, and results in the surface atoms being quasithreefold coordinated to second-layer atoms. A simple model for the driving force for this reconstruction has been proposed.[14,15] However, some very subtle factors must be operative since Mo(011) was not observed to reconstruct.[15] In addition, the work-function changes upon hydrogen adsorption are qualitatively different. On W(011), it *decreases* monotonically with an approximately linear dependence upon hydrogen coverage, reaching a saturation change of -450 meV.[16] On Mo(011), however, it *increases* nearly linearly with coverage up to half a monolayer, where the change is just $+70$ meV.[17] For higher coverages, it falls slightly. These changes are related to the changing surface dipole which is partly determined by and ultimately screened by the Fermi-surface electrons. Part of our motivation is to understand the nonintuitive differences between these two otherwise similar surfaces.

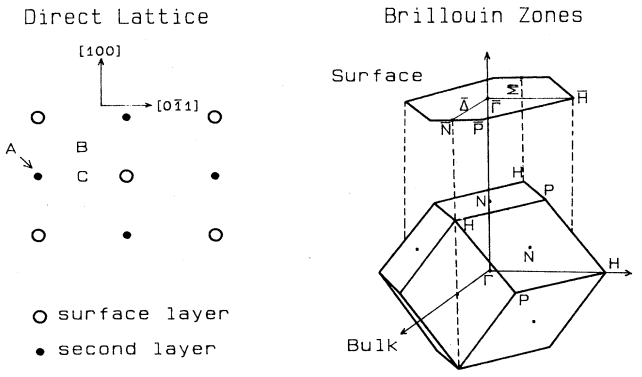

FIG. 1. Schematic of the body-centered-cubic (011) surface unit net (left) and the surface and bulk Brillouin zones (right). The hydrogen adsorption sites which have been suggested are the long bridge or hourglass site (A), a quasithreefold site labeled B, and the short bridge labeled C.

The format of this paper is as follows. In the next section, we describe our experimental procedures. The following section gives our experimental results for the clean and hydrogen-covered Fermi surfaces and discusses them in light of the three-dimensional Fermi surface projected onto the surface Brillouin zone. The final section analyzes the results in terms of their significance to other static and dynamical surface properties.

II. EXPERIMENTAL TECHNIQUES

A $>99.99\%$-purity Mo(011) crystal 1 cm in diameter was oriented normal to the [011] bulk crystalline axis by Laue x-ray backreflection to within $<0.5°$. A 1.5-mm-thick slice was cut and electromechanically polished in 15 vol % sulfuric acid in methanol to a lustrous finish, and inserted into our vacuum system. After several cycles of oxidation at 1300–1500 K followed by sublimation of the oxide at 2300 K, an exceptionally clean and well-ordered surface was obtained as determined by low-energy electron diffraction and Auger-electron spectroscopy. The operating pressure of $(0.8–1.2)\times10^{-10}$ torr was sufficient to maintain a clean surface for 15–20 min, as determined by the gradual disappearance of some of the more contamination-sensitive features in our spectra. These could easily be restored by thermally desorbing residual hydrogen and carbon monoxide from the surface. This desorption procedure could be performed repeatedly for several days without degradation of the surface.

Where required to determine the surface sensitivity of certain spectral features, the room-temperature surface was exposed to hydrogen gas in the form of H_2, either by back-filling the chamber or by placing the sample in the line of sight of a channel-plate array doser.

The ARP experimental system has been described previously.[18,19] High angular and energy resolution experiments can be performed readily in this system. For the experiments described here, the total instrumental resolution was always less than 80 meV full width at half maximum (FWHM), and the full angular acceptance was 1° or better. Experiments were performed at the National Synchrotron Light Source at Brookhaven National Laboratory (Upton, NY), using a 6-m toroidal-grating monochromator. Spectra could be accumulated with adequate signal-to-noise ratio under these conditions in typically 2–5 min.

III. EXPERIMENTAL RESULTS

The procedure for determining a Fermi surface for surface-localized states using ARP is straightforward, albeit somewhat tedious. In a given experiment, we typically fix the incident-photon energy and electron-emission angles to produce an electron energy-distribution curve (EDC). The first step is to determine which spectral features in these curves are related to the surface. As explained elsewhere,[20] we use various experimental tests which help to distinguish surface states and resonances from bulk states. Features which are particularly sensitive to hydrogen adsorption, either by shifting in energy or by being extinguished, are conditionally identified as either surface states or resonances. We also check to ensure that these do not disperse with momentum normal to the surface. Finally and most importantly in the present work, we distinguish those features which lie in a projected bulk band gap as surface states. We have the advantage in these studies of knowing the bulk Fermi surface accurately[21] (see below), so that this test has proven to be quite useful. Generally, once a segment of 2D Fermi surface has been located, we do not perform these tests at every momentum.

A. Clean surface

Using energy- and parallel-momentum-conservation relations, we can determine in a very straightforward fashion a 2D dispersion relation and thus the Fermi surface for surface-localized states.[9–11] Two series of EDC's collected from clean Mo(011) along lines parallel to the $\bar{\Delta}$ and $\bar{\Sigma}$ lines of the surface Brillouin zone (SBZ) are presented in Fig. 2 (see Fig. 1 for a designation of symmetry points and lines). Each of these intersects a segment of the complete Fermi surface shown in Fig. 3. Thus a feature in the spectra near the Fermi level abruptly disappears as the parallel momentum is varied. These data could easily be plotted on dispersion curves, as was done previously for similar data collected along the symmetry lines.[20] We are interested in determining where the bands cross the Fermi level, and the two series thus yield the points labeled *A* and *B* in Fig. 3. Once crossings such as these are found, we trace the complete Fermi surface by moving in small increments of k space at a time without a systematic determination of complete dispersion relations. This reduces the total number of spectra needed to determine a complete Fermi surface. A further reduction is attained by working primarily in one irreducible wedge of the SBZ and simply performing checks in other parts of the zone only to ensure symmetry. In spite of this reduction, however, the data in Figs. 3(a) and 3(b) required over 1000 EDC's to achieve an internally consistent data set.

We acknowledge that the finite linewidths observed in Fig. 2 result in some ambiguity in accurately locating the momentum where the surface features actually cross the Fermi level. This results in an ultimate accuracy of ± 0.03 Å^{-1} and a precision of ± 0.02 Å^{-1}. As mentioned earlier, this accuracy is not as good as that attained by the techniques used for bulk Fermi-surface measurements. Most of this uncertainty is systematic in nature, so that the shapes of the 2D Fermi-surface segments we derive are essentially correct while their sizes may be slightly in error. This accuracy could probably be improved somewhat by performing more complete extrapolations of surface bands to the Fermi level.

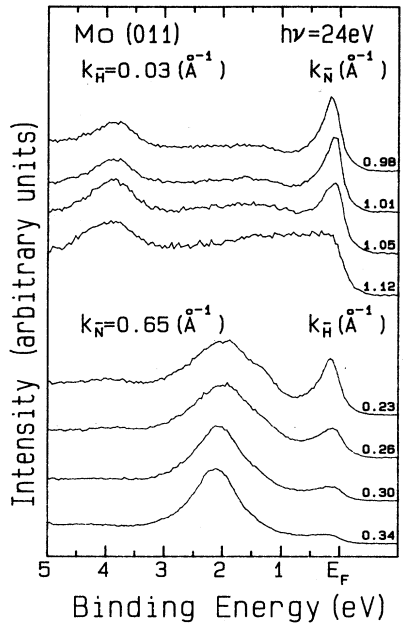

FIG. 2. ARP EDC's collected along lines parallel to the $\bar{\Delta}$ and $\bar{\Sigma}$ lines of the surface Brillouin zone in the vicinity of the Fermi-surface crossings labeled *A* and *B* in Fig. 3. Note the abrupt disappearance of the features near E_F as a function of parallel momentum.

The data shown in Figs. 3(a) and 3(b) clearly indicate that there are four closed Fermi-surface orbits on the clean surface. As discussed below, three of these are hole pockets and one is an electron pocket. Also shown in

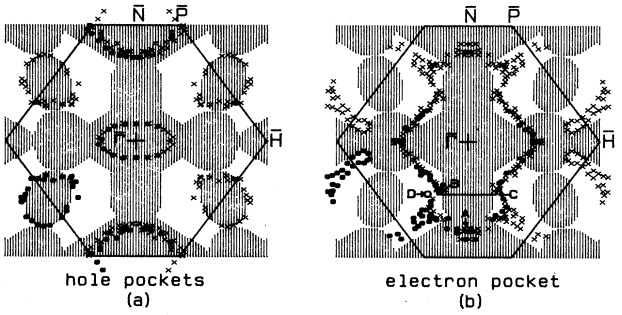

FIG. 3. Fermi-surface orbits for (a) the three hole ellipses and (b) the complex electron pocket observed on clean Mo(011). The solid dots are real data while the crosses have been produced by mirror-plane symmetry. The shaded regions are the projected bulk Fermi surface, calculated as explained in the text.

Figs. 3(a) and 3(b) is the bulk molybdenum Fermi surface projected onto the SBZ. This was calculated using a nonorthogonal tight-binding interpolation scheme.[22] This calculation reproduces fairly accurately the measured bulk Fermi surface,[21] while at the same time allowing us the flexibility to vary the projected energy arbitrarily. We have not included the spin-orbit interaction in this calculation. The most significant change its inclusion would introduce would be that the segments at $k_{\parallel} \approx 1.0$ Å^{-1} along $\bar{\Sigma}$ would not contact.[23]

1. Hole ellipses

The three roughly elliptical orbits shown in Fig. 3(a) centered at the $\bar{\Gamma}$ point and along both of the SBZ boundary lines are hole orbits in the sense that they enclose unoccupied levels. They are observed to orbit three distinct projections of the same bulk hole ellipsoid centered at the N points of the bulk Brillouin zone.[21] Two of the surface hole orbits are degenerate with the projections of other segments of the bulk Fermi surface and are thus accurately called surface resonances. The hole orbit near the zone center is embedded in the projection of the bulk electron jack, while the hole orbit near the $\bar{N}$ point is embedded in the projection of the bulk hole octahedron centered at the bulk H points. The third hole orbit appears to be a true surface state given that the calculation overestimates the size of the bulk ellipsoid slightly. We do not observe any systematic broadening of the features forming resonant orbits over those forming the orbit which is a true state, indicating that the resonant coupling to bulk states must not be particularly large. This point will be further addressed in a forthcoming article.[24] These hole orbits are similar in all respects to those observed previously on W(011).[13]

2. Electron orbit

The final surface orbit is an electron orbit centered on the $\bar{\Gamma}$ point. It is irregular in shape, but is seen more or less to encompass the projection of the bulk electron jack onto the SBZ. Away from the symmetry lines, the electron orbit is a true state, while near these it is resonant with bulk states. As explained previously,[20] the bulk continua along the symmetry lines in which this orbit is embedded are of the opposite nominal mirror-plane symmetry. In the absence of the spin-orbit interaction and precisely along the symmetry lines, the orbit would exist in a symmetry gap and would thus be a true state. As for the hole orbits, the resonant coupling to the bulk continuum must not be particularly strong. The regions where the electron pocket is resonant with bulk states do produce experimental difficulties, however, since the bulk states normally produce a broad feature at the Fermi level which must be discriminated.

This electron orbit is different in shape than that observed on W(011).[13] For molybdenum it is more extended along $\bar{\Delta}$ but less extended along $\bar{\Sigma}$ than for tungsten. An accurate description of the narrow segments extending into the second Brillouin zone near the $(\bar{H},\bar{P})$ points was particularly difficult to attain since the band is never very far below the Fermi level in this region. Given the necessity to flash our surface clean periodically, there is a competition between waiting long enough for the crystal to cool so that the Fermi surface is not thermally smeared, and accumulating spectra quickly enough so that the modifications by hydrogen adsorption reported below do not perturb the observed result. We were careful to eliminate these systematic errors, and believe that the narrow segment is accurately reproduced in our data.

A significant complication in accumulating the complete Fermi surface shown in Fig. 3 is the large intensity asymmetries often observed in rotating on opposite sides of a mirror plane perpendicular to the horizontal plane defined by the polarization vector and the surface normal. An example is shown in Fig. 4, which shows momentum-equivalent Fermi-surface crossings for the electron pocket taken with different photon polarizations. In these EDC's, the crystal was oriented with the $\bar{\Delta}$-axis vertical. Spectra are shown on opposite sides of this mirror plane as a function of component of momentum parallel to $\bar{\Sigma}$. In this particular case, the peak corresponding to the electron pocket crosses the Fermi level at $k_{\parallel} \approx 0.25$ Å^{-1}, labeled D in Fig. 3. This feature is quite intense when rotating toward the polarization vector, but is very weak when rotating away from it. Other bands on this surface show exactly the inverted behavior. We have not been able to derive any useful information from this

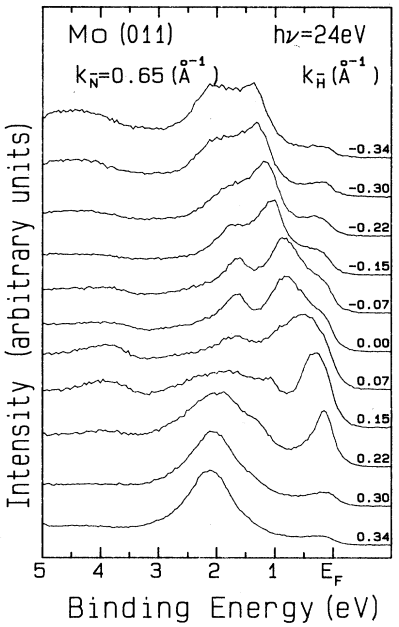

FIG. 4. Momentum-equivalent sets of EDC's showing the marked asymmetry in rotating the electron-emission direction on opposite sides of a mirror plane, either toward or away from the photon polarization vector. The observed Fermi-level crossing occurs at the point labeled C in Fig. 3. In this case, much higher precision can be achieved in determining k_F by scanning toward the polarization vector.

asymmetry. Similar results on W(001) have been interpreted as an interference between emission amplitudes excited with the in-plane and out-of-plane components of the polarization vector.[25] We have found it best to trace some segments of the Fermi surface in different symmetry-related wedges of the SBZ. In Fig. 3, the "original" data are indicated by solid circles, while the points which have been deduced by mirror-plane symmetry are indicated by crosses.

3. *Relation to previous results*

It is enlightening to draw a connection between our earlier results[20] for the surface bands along the symmetry lines and the results shown in Fig. 2. We reproduce in Fig. 5 the appropriate figure from our earlier paper which summarizes the bands along the $\bar{\Delta}$ and $\bar{\Sigma}$ lines on a projection of the bulk band structure. In this figure, we identified three Fermi-surface crossings in each mirror plane. Since the $\bar{P}$ and $\bar{H}$ points are equivalent by reciprocal-lattice symmetry, these crossings are clearly identified with those points on the complete Fermi surface in Fig. 3 along the symmetry lines. Without determining the complete Fermi surface, it would not be obvious that the crossings observed in Fig. 5 should connect as shown in Fig. 3. The near degeneracy of the two bands near 1.0 Å^{-1} along $\bar{\Delta}$ in Fig. 5 is in fact clarified by the Fermi surface, since these are seen to arise from different orbits which follow different trajectories away from the symmetry line.

B. Hydrogen-covered surface

The previous article[20] demonstrated and interpreted the differing sensitivities to hydrogen adsorption of the surface bands shown in Fig. 5. These can be categorized by those which are effectively quenched by hydrogen and those which simply shift downward in energy. Not surprisingly, this distinction is preserved and even magnified in measuring the effect of hydrogen upon the various surface orbits. All three of the hole orbits are rapidly quenched by small quantities of hydrogen. The fact that all three hole orbits show the same sensitivity is perhaps not surprising. They apparently all are split from the same ellipsoidal segment of the projected bulk Fermi surface, and thus to a first approximation would be composed of similar localized orbitals. They might therefore be expected to have similar sensitivities to adsorption, as observed.[26]

The bands which were observed to shift downward upon hydrogen adsorption in the previous study are those which are connected by the electron pocket in Fig. 3. We might anticipate that this pocket would expand in area upon adsorbing hydrogen. This is precisely what is observed. As was observed on W(011),[13] the pocket expands and merges with its counterpart in the second Brillouin zone at some small but finite hydrogen coverage. As shown in Fig. 6, at saturation, two distinct hole orbits remain, centered on the two edges of the SBZ. While the clean-surface electron pocket was observed to be somewhat different from that of W(011), the results from the saturated surfaces are remarkably similar. The hole orbits which are left are qualitatively similar to two of the hole orbits observed on the clean surface, but quantitatively different. The orbits at saturation coverage lie largely within projected Fermi-surface band gaps and are thus truly surface states characteristic of Mo(011)+H. It is important to note that this merging occurs in the vicinity of the $\bar{\Sigma}$ line where the spin-orbit interaction has a pronounced effect on the projected bulk Fermi surface. Attempts to calculate the observed modification to the

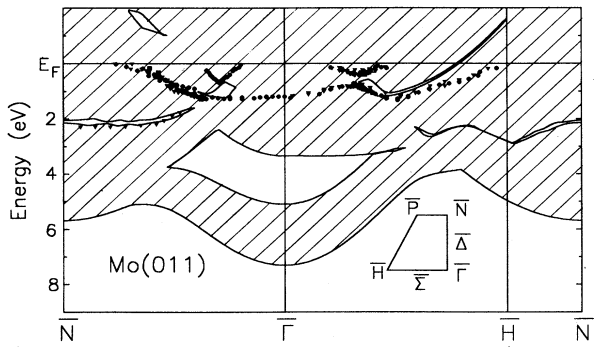

FIG. 5. Summary of our experimental surface energy bands along the $\bar{\Delta}$ and $\bar{\Sigma}$ lines plotted on a projection of the bulk molybdenum band structure taken from Ref. 20. The calculation includes the spin-orbit interaction, so that mirror-plane symmetry need not be considered. The data were taken at the following photon energies: ●, $h\nu=24$ eV; ▲, $h\nu=40$ eV; ▼, $h\nu=50$ eV; ■, $h\nu=60$ eV.

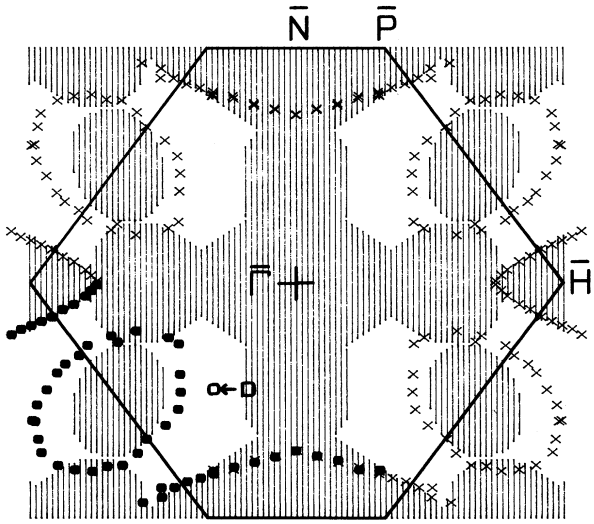

FIG. 6. Fermi-surface orbits for the two hole ellipses observed on hydrogen-saturated Mo(011), plotted on the projected bulk Fermi surface. The solid dots are real data while the crosses have been produced by mirror-plane symmetry. As explained in the text, these ellipses are derived from the electron pocket in Fig. 3(b).

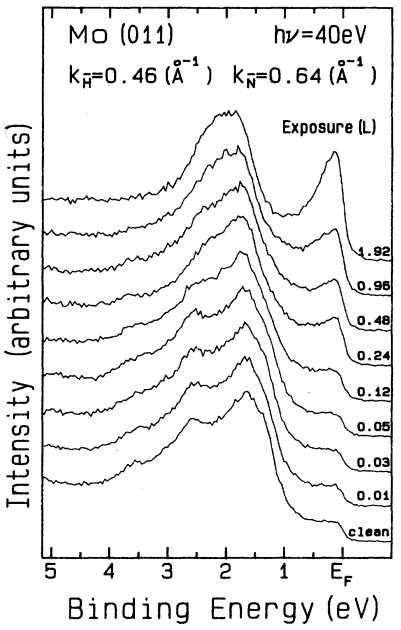

FIG. 7. EDC's collected as a function of hydrogen dose at the point labeled *D* in Figs. 3 and 6. Note that a peak grows in near the Fermi level as hydrogen is adsorbed and the electron pocket shifts outward.

surface Fermi surface may require inclusion of this relativistic effect.

A useful view of these modifications to the Fermi surface is attained by collecting spectra as a function of hydrogen dose at a point outside the clean-surface electron orbit and the saturation hole orbits. We expect to observe a peak grow in near the Fermi level. This is observed in the EDC's shown in Fig. 7, which were collected at the point labeled *D* in Figs. 3 and 6.

Ideally, we would determine the complete Fermi surface at intermediate hydrogen coverages so as to produce

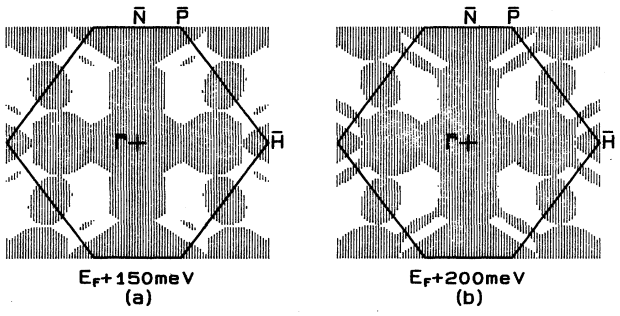

FIG. 8. Projections of the bulk molybdenum Fermi surface onto the (011) surface Brillouin zone at energies (a) 150 meV and (b) 200 meV above the Fermi level. Note that the projection of the bulk electron jack grows markedly and merges with its counterpart in the second zone, similar to what is observed for our surface orbit in Figs. 3 and 6.

a detailed analysis of the changes observed. This is very difficult experimentally since the time required to determine a complete Fermi surface is very large compared to the length of time that a partially covered surface is stable in our vacuum system. What we have done instead is to determine the change of the Fermi wave vector as a function of hydrogen dose along a few lines in the SBZ. A sample of these results is shown in Fig. 8. This plots the fractional changes in both the work function and the Fermi wave vector along a line parallel to $\bar{\Sigma}$ and passing through the point labeled *D* in Figs. 3 and 6 as a function of hydrogen dose. The shifts are observed to be continuous and appear to be related to one another, as explained below.

IV. DISCUSSION

A. Electronic structure and hybridization

The Fermi surfaces presented in Figs. 3 and 6 are of interest in part purely from the perspective of surface electronic structure. Loosely speaking, we can think of molybdenum and tungsten as partially covalent metals. In a tight-binding model, forming a surface breaks bonds between atoms. The resulting dangling bonds can form well-defined surface bands which lie in or near projected band gaps. The hybridization at the Fermi level between these bands is clearly apparent in Fig. 3. This is manifested by the intricate way in which the irregularly shaped electron pocket threads its way through the hole ellipses.

The bands which form the hole ellipses are quenched by hydrogen, so that these bands must be composed of dangling bonds which are very labile. Our hypothesis is that these bonds are directed toward the hydrogen atoms in their equilibrium adsorption site, and are intimately involved in forming the adsorption bond. Elsewhere, we have elaborated upon this idea and concluded that hydrogen sits in or near the long bridge site (sites labeled *A* and *B* in Fig. 1),[26] as is thought to be the case on W(011).[27] The data presented in Fig. 6 could probably be coupled to first-principles calculations to deduce the hydrogen adsorption geometry with some precision.

Previously, we presented evidence that upon adsorption the electrons in the labile dangling bond states end up in H—Mo bonding orbitals. We see more evidence for this in Figs. 3 and 6. As the hole bands are removed by hydrogen, the restrictions due to band hybridization are relieved and the electron pocket grows into the region previously occupied by the hole ellipses. If the electrons in the hole pockets were attenuated simply because hydrogen scattered them strongly without changing their energy very much, we would probably not observe such a dramatic change in the electron orbit.

B. Changes in the electron pocket

The changes which the electron pocket undergoes deserve special attention, since similar Fermi-surface changes are difficult to observe in bulk media. The changes are usefully compared to a rigid-band model

which is often used as a simple model for the density of states of a dilute alloy.[28] The difference here is that, instead of changing the density of electrons in the whole system, we are filling a particular surface band by lowering its energy relative to a fixed Fermi energy. A convenient way to view this comparison is to project the bulk band structure onto the SBZ at energies slightly removed from the calculated bulk Fermi level. This is shown in Figs. 8(a) and 8(b) where we have projected at energies 150 and 200 meV *above* the Fermi level, respectively. We see in this figure that the projection of the bulk electron jack expands and merges with its counterpart in the second Brillouin zone in much the same way as does our surface electron orbit. Experimentally, we measure a *downward* energy shift in the surface band by roughly 200 meV, depending on the position in the Brillouin zone. This rough equivalence justifies our analogy to the rigid-band model.

Electrons at the Fermi surface are the most polarizable in a metal. They are, for instance, intimately involved in screening external potentials. For this reason, we might expect our results to be related in some way to properties of the surface which depend on this polarizability. The most obvious property with which to compare is the change in work function since this gives a crude measure of the changes in the surface dipole layer. That the changes we observe in the electron orbit are related to the changes in work function is strongly suggested by the results shown in Fig. 9. The functional dependence of these quantities is very similar, indicating that they are likely to be related. It appears that the electrons at the Fermi level are indeed responding to changes in the surface dipole layer.

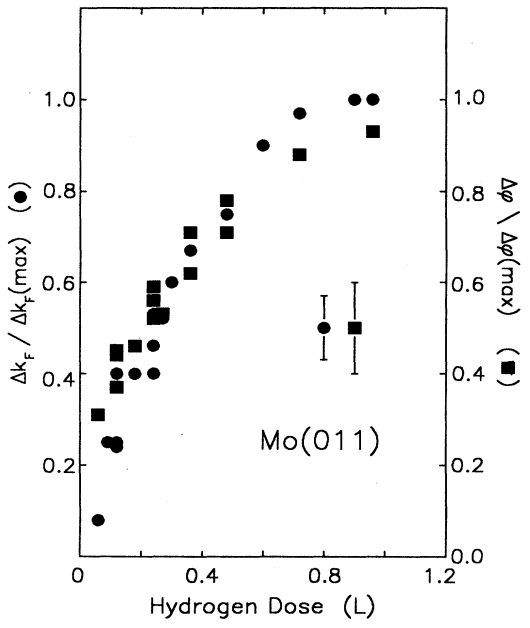

FIG. 9. Fractional change in the Fermi wave vector and the work function as a function of hydrogen dose. The measurements of the Fermi wave vector were performed along a line parallel to $\bar{\Sigma}$ passing through the point labeled *D* in Figs. 3 and 6. Note the marked similarity between the behavior of the Fermi surface and the work function. [1 langmuir (L) $\equiv 10^{-6}$ torr s.]

In order to make this relationship between the observed change in Fermi surface and the work function definitive, we would need to know both the amount of hydrogen-induced charge transfer in the vicinity of the surface and its spatial distribution. The first of these is simple if we ignore the possibility of transferring charge into the bulk via the resonant portions of the Fermi surface. We simply measure the fractional area of the electron pocket enclosed within the first Brillouin zone and multiply by 2 for the spin degeneracy. The total amount of charge transferred into the band is 0.60 ± 0.05 electrons per atom. We cannot easily measure the spatial distribution of this charge, but in order to produce the observed maximum work function change of $+70$ meV, the centroid of the charge distribution would need to shift outward from the surface by only ≈ 0.005 Å. This small length indicates just how significant the charge we measure might be.

As mentioned previously, the Fermi-surface changes we have observed on Mo(011) are fairly similar to those reported previously on W(011).[13] Moreover, a qualitatively similar relationship was observed between the work-function change and the changes in Fermi wave vector. As mentioned in the Introduction, however, the work-function changes on these two surfaces upon hydrogen adsorption are opposite in sign. Lacking knowledge of the location of the centroid of the hydrogen-induced surface charge density, this enigma is difficult to explain. It suggests that the relationship between the Fermi-surface modifications and work-function change might not be as direct as our previous discussion suggests. The arguments presented above concerning healing dangling bonds and relieving band hybridization would produce the observed Fermi-surface changes regardless of the work-function change. This might in fact be the link between the changes in work function and Fermi surface. Further theoretical work will be required to explain this enigma.

The continuous nature of the changes in band energies, Fermi surface, and work function deserves further consideration. The abrupt disappearance of some surface features (i.e., a successful "crud" test) can be easily understood. The adsorbate interacts strongly with the surface state electrons and these are swept out of the gap. This can occur either through a direct chemical-bonding interaction, or simply due to the significant change in boundary conditions at the surface induced by the adsorbate.

The case of "weak" interaction, where the surface band shifts continuously with coverage, can be understood qualitatively as well. For a perfect, clean surface, the surface-state wave function is an extended Bloch state with well-defined momentum parallel to the surface. On this surface at room temperature, the adsorbate is disordered and, strictly speaking, the momentum is not well defined. By assumption, however, the Bloch wave is not strongly scattered by the adsorbate centers. We can

think of eigenstates which are relatively narrow momentum-space wave packets centered on the bands for the perfect surface. This is consistent with the broadened features observed in spectra of the contaminated surface. The scattering centers can also energetically perturb the delocalized Bloch state. In this case the energy of the broadened bands will be shifted to an extent which depends on the coverage. Unfortunately, there is no theoretical treatment which provides a more quantitative treatment of the relationship between monotonic changes in band energies and Fermi surfaces and other properties such as work-function change.

C. Phonon anomalies and reconstruction

The dynamical coupling between electronic and vibrational degrees of freedom in a metallic system is one of the most important aspects of metal physics. This coupling is necessarily determined in part by the Fermi-surface contours. One important manifestation of this coupling is the Kohn anomalies mentioned in the Introduction. Without knowledge of the matrix elements which govern the electron-phonon coupling, we cannot predict the strength of a particular anomaly. We can, however, predict momenta at which several of these might be observed from the data in Figs. 3 and 6. More importantly, we predict that the character of these anomalies will be dramatically affected by hydrogen adsorption.

The Kohn anomalies can be separated into two classes, those that couple two points on one orbit and those that couple points on different orbits. The former are similar to the screening anomalies which occur at $2k_F$ in the free-electron gas. A simple example observed in Fig. 3(a) is at points on the symmetry lines on opposite sides of hole ellipses centered at $\bar{\Gamma}$ And $\bar{N}$. Tangents to these points are parallel, so that a low-energy excitation with a momentum which spans these points would be efficiently coupled to the electron-hole–pair continuum. The excitation would thus be damped and a Kohn anomaly would result. A good example of the latter type of anomaly exists on the saturated surface. Here, the points on the two hole pockets along the $\bar{P}$–$\bar{H}$ line have parallel tangents and enhanced intraband damping would result.

Several other anomalies can be predicted from inspection of Figs. 3 and 6. We have enumerated in Table I some of the more pronounced Kohn anomalies which might occur along the lines of high symmetry in the SBZ. These are classified by their 2D wave vector, the orbits which they couple, and by a crude measure of the strength of the screening singularity. We use for this measure the inverse of the difference in curvature of the nested segments of the Fermi surface. This neglects completely all matrix element effects. Density-of-states effects are included, however, in such a way that the larger the number in the third column of the table, the stronger the singularity might be.

Our previous work on W(011) predicted significant damping of the zone-center symmetric-stretch hydrogen mode due to coupling to intraband excitations. A similar effect should occur on Mo(011). The reasoning which leads to this prediction is simple. As the hydrogen layer vibrates uniformly normal to the surface, the surface dipole changes, thereby modifying the work function. Figure 9 implies that the electron pocket will fill or empty as well, resulting in electronic damping. A very similar dynamical response of the electrons near the Fermi level was predicted in a recent calculation for the W(001)-(2H) system.[29] Note that this damping occurs only for a uniform displacement of the hydrogen layer, i.e., for the zone-center phonon mode. A similar mechanism was invoked to explain the damping of molecular vibrations at a surface.[30]

The final aspect of interest in our data is the relationship to surface reconstruction. As mentioned in the Introduction, W(011) has been observed to undergo a (1×1) displacive reconstruction upon addition of roughly 0.5 monolayers of hydrogen, while Mo(011) has not. From the point of view of the Fermi surface, we need to look for anomalies at zero momentum since the reconstruction involves a uniform displacement of the outermost layer. When two segments of Fermi surface touch, a new coupling channel is opened at $\mathbf{q}=(0,0)$. This aspect of our data could conceivably play a role in helping to drive the reconstruction. However, in both molybdenum and in tungsten, the electron pocket merges with its second-Brillouin-zone counterpart at a coverage of only ≈ 0.2 monolayers, or well below that required to produce the reconstruction. Moreover, the merging is fairly similar in the two metals, while the reconstructive properties are not. Further theoretical work will clarify the influence of the Fermi surface on the reconstruction observed on W(011).

TABLE I. Some of the more pronounced Kohn anomalies predicted from our data. The orbits are labeled E for the electron orbit, $H1$ and $H2$ for the clean-surface hole orbits which surround the $\bar{\Gamma}$ and $\bar{N}$ points, and HA and HB for the larger and smaller hydrogen-covered surface hole orbits. The momentum is given in Å^{-1} by its components parallel and perpendicular to $\bar{\Sigma}$ and $\bar{\Delta}$, respectively. The strength parameter is explained in the text and has units of Å^{-1}.

Surface	$\mathbf{q}=(q_{\bar{\Sigma}},q_{\bar{\Delta}})$	Orbits	Strength
clean	(0.00,0.43)	$H1$-$H1$	0.62
clean	(0.00,0.74)	$H2$-$H2$	0.38
clean	(0.00,2.22)	E-E	0.30
clean	(0.83,0.00)	$H1$-$H1$	0.08
clean	(0.96,0.00)	$H2$-$H2$	0.24
clean	(1.52,0.00)	E-E	0.17
clean	(0.00,1.33)	$H1$-E	0.20
clean	(0.00,1.26)	$H1$-$H2$	0.98
clean	(0.00,0.07)	$H2$-E	0.25
clean	(1.18,0.00)	$H1$-E	0.16
clean	(2.27,0.00)	$H2$-E	0.55
H-saturated	(0.00,0.74)	HA-HA	1.03
H-saturated	(2.30,0.00)	HA-HA	0.10
H-saturated	(0.35,0.53)	HB-HB	0.54
H-saturated	(0.19,0.24)	HA-HB	0.31

V. SUMMARY AND CONCLUSIONS

We have determined experimentally the complete Fermi surface of clean and hydrogen-covered Mo(011) and investigated its ramifications. Detailed experiments such as this provide a very detailed look at the chemisorption bond both from a static and dynamic point of view. To date, surface states have not been shown definitively to determine other dynamical properties of a surface. Accurate measurements of surface-phonon dispersion relations for this surface and for W(011) may provide evidence for this. Future studies will include investigating the effect of adsorbate electronegativity and strained overlayers on the Fermi surfaces of 2D systems with a goal of further probing the relation between surface dynamical and geometrical structures.

ACKNOWLEDGMENTS

This work was carried out in part at the NSLS at Brookhaven National Laboratory (Upton, NY) which is supported by the U.S. Department of Energy (DOE) (Division of Materials Science and Division of Chemical Sciences of the Office of Basic Energy Sciences). Financial support from the U.S. DOE under Grant No. DE-FG06-86ER45275 and from donors of the Petroleum Research Fund, administered by the American Chemical Society, is gratefully acknowledged. One of us (S.D.K) gratefully acknowledges partial financial support by the Alfred P. Sloan Foundation and by the National Science Foundation.

---

*Present address: National Synchrotron Light Source, Brookhaven National Laboratory, Bldg. 725A/U3, Upton, NY 11973-5000.

[1] *Electrons at the Fermi Surface,* edited by M. Springfield (Cambridge University Press, Cambridge, 1980).

[2] J. A. Wilson, F. J. Di Salvo, and S. Mahajan, Adv. Phys. **24**, 117 (1975).

[3] E. Tossatti and P. W. Anderson, Jpn. J. Appl. Phys. Suppl. **2**, Pt. **2**, 381 (1974).

[4] X. W. Wang, C. T. Chan, K. M. Ho, and W. Weber, Phys. Rev. Lett. **60**, 2066 (1988).

[5] W. Kohn, Phys. Rev. Lett. **2**, 393 (1959).

[6] M. Persson and B. Hellsing, Phys. Rev. Lett. **49**, 662 (1982).

[7] U. Harten, J. P. Toennies, C. Wohl, and G. Zhang, Phys. Rev. Lett. **55**, 2308 (1985).

[8] G. Benedek, G. Brusdeylins, C. Heimlich, L. Miglio, J. G. Skofronick, J. P. Toennies, and R. Vollmer, Phys. Rev. Lett. **60**, 1037 (1988).

[9] E. W. Plummer and W. Eberhardt, *Advances in Chemical Physics* (Wiley, New York, 1982), Vol. 49.

[10] F. J. Himpsel, Adv. Phys. **32**, 1 (1985).

[11] *Electronic Properties of Surfaces,* edited by M. Prutton (Hilgaer, Bristol, 1984).

[12] J. C. Campuzano, J. E. Inglesfield, D. A. King, and C. Somerton, J. Phys. C **14**, 3099 (1981).

[13] R. H. Gaylord, K. Jeong, and S. D. Kevan (unpublished).

[14] J. W. Chung, S. C. Ying, and P. J. Estrup, Phys. Rev. Lett. **56**, 749 (1986).

[15] M. Altmann, J. W. Chung, P. J. Estrup, J. M. Kosterlitz, J. Prybyla, D. Sahu, and S. C. Ying, J. Vac. Sci. Technol. **5**, 1045 (1987).

[16] D. D. Barford and R. R. Rye, J. Chem. Phys. **60**, 1046 (1974).

[17] M. L. Ernst-Vidalis, M. Kamaratos, and C. Papageorgopoulos, Surf. Sci. **189**, 276 (1987).

[18] S. D. Kevan, Rev. Sci. Instrum. **54**, 1441 (1983).

[19] P. Thiry, P. A. Bennett, S. D. Kevan, W. A. Royer, E. E. Chaban, J. E. Rowe, and N. V. Smith, Nucl. Instrum. Methods **222**, 85 (1984).

[20] K. Jeong, R. H. Gaylord, and S. D. Kevan, Phys. Rev. B **38**, 10 302 (1988).

[21] D. M. Sparlin and J. A. Marcus, Phys. Rev. **144**, 484 (1966).

[22] D. A. Papaconstantopoulos, *Handbook of the Band Structure of Elemental Solids* (Plenum, New York, 1986).

[23] L. F. Mattheiss and R. E. Watson, Phys. Rev. Lett. **13**, 526 (1964).

[24] S. Dhar and S. D. Kevan (unpublished).

[25] S.-L. Wang, E. W. Plummer, and T. Gustaffson, Phys. Rev. B **18**, 1718 (1978).

[26] K. Jeong, R. H. Gaylord, and S. D. Kevan (unpublished).

[27] G. B. Blanchet, N. J. DiNardo, and E. W. Plummer, Surf. Sci. **118**, 496 (1982).

[28] N. F. Mott and H. Jones, *The Theory of the Properties of Metals and Alloys* (Dover, New York, 1958).

[29] R. Biswas and D. R. Hamann, Phys. Rev. Lett. **56**, 2291 (1986).

[30] B. N. J. Persson and R. Ryberg, Phys. Rev. Lett. **48**, 549 (1982).